Dark matter haloes in modified gravity and dark energy: interaction rate, small- and large-scale alignment

Benjamin L'Huillier,[1,2]★ Hans A. Winther,[3,4] David F. Mota,[5] Changbom Park[2] and Juhan Kim[6]

[1]*Korea Astronomy and Space Science Institute, Yuseong-gu, 776 Daedeok daero, 34055 Daejeon, Korea*
[2]*School of Physics, Korea Institute for Advanced Study, 85 Hoegi-ro, Dongdaemun-gu, Seoul 130-722, Korea*
[3]*Astrophysics, University of Oxford, DWB, Keble Road, Oxford OX1 3RH, UK*
[4]*Institute of Cosmology and Gravitation, University of Portsmouth, Portsmouth, Hampshire PO 3FX, UK*
[5]*Institute for Theoretical Astrophysics, University of Oslo, 0315 Oslo, Norway*
[6]*Center for Advanced Computation, Korea Institute for Advanced Study, 85 Hoegi-ro, Dongdaemun-gu, Seoul 130-722, Korea*

ABSTRACT

We study the properties of dark matter haloes in a wide range of modified gravity models, namely, $f(R)$, DGP and interacting dark energy models. We study the effects of modified gravity and dark energy on the internal properties of haloes, such as the spin and the structural parameters. We find that $f(R)$ gravity enhances the median value of the Bullock spin parameter, but could not detect such effects for DGP and coupled dark energy. $f(R)$ also yields a lower median sphericity and oblateness, while coupled dark energy has the opposite effect. However, these effects are very small. We then study the interaction rate of haloes in different gravity and find that only strongly coupled dark energy models enhance the interaction rate. We then quantify the enhancement of the alignment of the spins of interacting halo pairs by modified gravity. Finally, we study the alignment of the major axes of haloes with the large-scale structures. The alignment of the spins of interacting pairs of haloes in DGP and coupled dark energy models show no discrepancy with GR, while $f(R)$ shows a weaker alignment. Strongly coupled dark energy shows a stronger alignment of the halo shape with the large-scale structures.

Key words: methods: numerical – galaxies: haloes – galaxies: interactions – dark matter – large-scale structure of Universe – cosmology: theory.

1 INTRODUCTION

The discovery of the acceleration of the expansion of the Universe by Riess et al. (1998) and Perlmutter et al. (1998), as well as studies from the large-scale structures (e.g. Colless 1999) led to the emergence of the lambda cold dark matter (ΛCDM) model, where the Universe is dominated by dark energy (DE), responsible for the acceleration of the expansion, and a CDM component that drives structure formation.

However, the nature of dark matter and DE is one of the main puzzles in modern physics. While there are many plausible candidates for dark matter, DE poses more theoretical challenges. The simplest choice is DE being due to vacuum energy in the form of a cosmological constant in Einstein's field equations. This model is in perfect agreement with current observations but is plagued by the fine-tuning problem.

The next to simplest option is that DE is dynamical, as in quintessence models. The DE fields can also have interactions with the dark matter sector, giving rise to interacting DE models (coupled quintessence; Amendola 2000). In these scenarios, there is no interaction between DE and baryons, as such the constraints coming from local gravity experiments are not applicable. Nevertheless, there are several cosmological bounds for these models specially coming from structure formation (Koivisto 2005; Mota et al. 2007; Mota, Shaw & Silk 2008; Pettorino 2013; Leithes et al. 2016, see Copeland, Sami & Tsujikawa 2006 for a review on DE).

Another possibility is that general relativity (GR) does not describe gravity properly on cosmological scales (Clifton et al. 2012). To get around the tight constraints coming from high-precision experiments on Earth and in the Solar system (Will 2006, 2014), viable modified gravity (MG) models must have some form of screening mechanism (Khoury 2010) to hide the modifications in the high-density regimes (relative to the cosmic mean) where these experiments have been performed.

In the recent years, both analytical and numerical studies of MG and screening mechanisms have become increasingly

★ E-mail: lhuillier@kias.re.kr

performed (Koivisto & Mota 2007; Gannouji et al. 2010; Mota, Sandstad & Zlosnik 2010; Li 2011; Li, Mota & Barrow 2011; Llinares & Mota 2013a,b; Llinares, Mota & Winther 2014; Winther et al. 2015). Not just because of it being a possible DE candidate, but also due to the fact that we are finally in the position where we can make precision, percent level, tests of GR on cosmological scales just as we have done in the Solar system in the last century. By studying alternatives to GR, we can find new ways of testing gravity on scales we have not tested it before, for instance via the study of the internal properties of haloes (Hellwing et al. 2013; Shi et al. 2015), the lensing mass (Zhao, Li & Koyama 2011), haloes in voids (Li, Zhao & Koyama 2012) or the three-points correlation function (Sabiu et al. 2016).

Studying halo formation in MG is thus important for two reasons. If gravity is not correctly described by GR, but by a modified theory, one needs to understand how MG affects galaxy formation. Moreover, galaxies and galaxy clusters themselves can be used as a test of gravity.

Future weak lensing surveys, such as Euclid (Laureijs et al. 2011; Amendola et al. 2013), will provide strong constrains on GR. However, the intrinsic alignment of galaxies will be a source of systematics. It is thus important to understand the alignment of galaxies in MG. Many groups have studied halo and galaxy alignment in ΛCDM (e.g. Hahn et al. 2007; Codis et al. 2012; Libeskind et al. 2013b) and Lee et al. (2013) studied the spin of dark matter haloes in MG.

L'Huillier, Park & Kim (2017) studied the effects of interactions on the small-scale alignment of haloes and their dependences with the environment, which was possible thanks to the large volume of the Horizon Run 4 (Kim et al. 2015). The interaction rate of haloes in the ΛCDM model was studied in L'Huillier, Park & Kim (2015).

In this paper, we use state-of-the-art *N*-body simulations of different MG and dark energy models, namely *f*(*R*), DGP and coupled DE, and study the internal properties of dark matter haloes, such as their structural and spin parameters, and external properties, such as their interaction rate, small-scale alignment with their interacting neighbour and large-scale alignment with the cosmic web.

The models are described in Section 2, and Section 3 presents the simulations we used and the method. Section 4 deals with the internal properties of haloes (spins and structural parameters), Section 5 studies interacting pairs, and Section 6 is devoted to the alignment with the large-scale structures.

2 GRAVITY MODELS

The main ingredient in a successful MG model is a screening mechanism that hides the modifications of gravity on Earth and in the Solar system, allowing it to pass the stringent constraints coming from local gravity experiments. The study of MG models, which may or may not be particularly interesting in their own right, can be thought of as a way of studying how the underlying screening mechanism work. Several different screening mechanisms are known in the literature (Joyce et al. 2015), and in this paper, we will consider two models, *f*(*R*) gravity and the normal branch DGP model, that have two different screening mechanisms in play: the chameleon and Vainhstein mechanism. For the chameleon mechanism (Khoury 2010), screening depends on the local value of the gravitational potential, while for the Vainshtein mechanism, screening is a function of the local matter density. Different screening mechanisms operating on non-linear scales may give rise to unique features. It is therefore highly desirable to explore observational consequences that help expose these differences using physical ob-

servables in the non-linear regime of structure formation. Below we will give a brief overview of the two models we consider in this paper. Both of these models have a background evolution that is either identical or very close to ΛCDM, so the differences in structure formation come solely from the addition of a fifth force that alters the growth of structures.

2.1 *f*(*R*) gravity

In *f*(*R*) gravity models (De Felice & Tsujikawa 2010), the Ricci scalar *R* is augmented by a general function *f*(*R*) given the action

$$S = \int \sqrt{-g}\,\mathrm{d}^4x \,\frac{M_{\mathrm{Pl}}^2}{2}\,[R + f(R)]\,, \tag{1}$$

where *g* is the determinant of the metric $g_{\mu\nu}$ and $M_{\mathrm{Pl}} \equiv 1/\sqrt{8\pi G}$.

The particular *f*(*R*) model studied in this paper is the so-called Hu–Sawicky model (Hu & Sawicki 2007) that is defined by

$$f(R) = -m^2\,\frac{c_1(-R/m^2)^n}{1 + c_2(-R/m^2)^n}\,, \tag{2}$$

where n, c_1, c_2 are dimensionless numbers satisfying $\frac{c_1}{c_2} = \frac{\Omega_\Lambda}{\Omega_m}$ and $m^2 = \Omega_m H_0^2$. In the high curvature regime $|R| \gg m$, we can write

$$f(R) \simeq -\frac{f_{R0}}{n}\,R_0\left(\frac{R_0}{R}\right)^n\,, \tag{3}$$

where R_0 (f_{R0}) is the present value of R ($f_R = \frac{\mathrm{d}f(R)}{\mathrm{d}R}$), respectively. For all the simulations in this paper $n = 1$, so the models are defined by a single dimensionless number f_{R0}. For the range of $|f_{R0}|$ values that we consider in this paper, the background evolution is almost indistinguishable from ΛCDM.

f(*R*) gravity can via a conformal transformation be written as a scalar–tensor theory where f_R plays the role of the scalar field (Brax et al. 2008). The equation determining the evolution of f_R is given by

$$\nabla^2 f_R = -\frac{a^2}{3}\left[\delta R + \frac{\delta\rho_m}{M_{\mathrm{Pl}}^2}\right] = -\frac{a^2}{3}\left[\sqrt{\frac{f_{R0}}{f_R}}R_0 - R(a) + \frac{\delta\rho_m}{M_{\mathrm{Pl}}^2}\right]\,, \tag{4}$$

where $\delta R = R - R(a)$ and $R(a)$ is the background value for R. In an *N*-body simulation of *f*(*R*) gravity, this equation is solved at every time-step to determine the fifth force $\frac{1}{2}\nabla f_R$.

The parameter f_{R0} controls the range of the scalar interaction and in the cosmological background today we have

$$\lambda_0 = 7.46 \times \sqrt{\frac{f_{R0}}{10^{-5}}}\,h^{-1}\mathrm{Mpc}\,. \tag{5}$$

Roughly speaking on large length-scales $r \gtrsim \lambda_0$ gravity behaves as GR, while on small scales $r \lesssim \lambda_0$ gravity is modified. In addition to this, we have a screening effect, the chameleon mechanism, in high-density regions. For objects that have a large Newtonian potential Φ_N, the fifth-force is suppressed by a factor $\left|\frac{3f_R}{2\Phi_N}\right|$. Thus, the parameter f_{R0} also acts as a critical potential; objects at the present time with $|\Phi_N| \gg |f_{R0}|$ do not feel any modification of gravity while objects with $|\Phi_N| \lesssim |f_{R0}|$ feel a modified Newton's constant $G_{\mathrm{eff}} = \frac{4}{3}G$.

2.2 DGP model

The DGP (Dvali, Gabadadze & Porrati 2000) model is a so-called braneworld model where our Universe is confined to a 4D brane

that is embedded in a 5D space–time. The action is given by

$$S = \int \sqrt{-g_{(4)}} \mathrm{d}^4 x \frac{R_{(4)}}{2} M_{\mathrm{Pl}(4)}^2 + \int \sqrt{-g_{(5)}} \mathrm{d}^5 x \frac{R_{(5)}}{2} M_{\mathrm{Pl}(5)}^2, \qquad (6)$$

where $g_{(4)}$ ($g_{(5)}$) denotes the metric on the brane (in the bulk) and $R_{(4)}$ ($R_{(5)}$) denotes the Ricci scalar on the brane (in the bulk). Since $M_{\mathrm{Pl}(4)} = 1/\sqrt{8\pi G}$, we only have one free parameter in the model that is usually expressed as the so-called cross-over scale $r_c = \frac{1}{2}\left(\frac{M_{\mathrm{Pl}(4)}}{M_{\mathrm{Pl}(5)}}\right)^2$.

The modifications of the gravity in the model is determined by a scalar-field ϕ, the brane-bending mode, which described how the brane we live on curves in the fifth-dimension. In a Friedmann–Lemaître–Robertson–Walker background, the gravitational potential, which determines how particles move in an N-body simulation, is given by $\Phi = \Phi_N + \frac{\phi}{2}$, where Φ_N is the standard Newtonian potential. The dynamics of ϕ in the quasi-static approximation is determined by

$$\nabla^2 \phi + \frac{r_c^2}{3\beta a^2}\left[(\nabla^2\phi)^2 - (\nabla_i\nabla_j\phi)^2\right] = \frac{a^2\delta\rho}{\beta M_{\mathrm{Pl}}^2}, \qquad (7)$$

where

$$\beta(a) = 1 + 2H(a)r_c\left(1 + \frac{\dot{H}(a)}{3H^2(a)}\right). \qquad (8)$$

The model we are working with here is the normal branch DGP model apposed to the original DGP model that had self-accelerating solutions. The latter one is effectively ruled out (Maartens & Koyama 2010). In the normal branch DGP model, the acceleration of the Universe is driven by a cosmological constant just as in ΛCDM. This model is a useful toy model to study the particular screening mechanism, the so-called Vainshtein mechanism, used by DGP to hide the modifications of gravity in local experiments. The modifications of gravity in the vicinity of a massive object of mass M and radius r_c are determined by a scale known as the Vainshtein radius $r_V \propto r_c^{2/3} M^{1/3}$. Test particles far outside the Vainshtein radius will feel a gravitational force that is enhanced, $G_{\mathrm{eff}} = G_N\left(1 + \frac{1}{3\beta(a)}\right)$, while test particles far inside the Vainshtein radius will just feel the standard Newtonian gravitational force $G_{\mathrm{eff}} \simeq G_N$. This basically means that we have screening in a region if the average matter density is higher than some critical value $\rho_{\mathrm{crit}} \simeq \frac{9\beta^2}{4(r_c H_0)^2}\rho_c$ where $\rho_c = 3H^2/8\pi G$ is the critical matter density in the Universe. For $\rho_m \gg \rho_{\mathrm{crit}}$, the fifth force is suppressed by a factor $\approx \sqrt{\rho_{\mathrm{crit}}/\rho_m}$.

2.3 Interacting DE

In interacting DE models (Wetterich 1995; Amendola 2000), the acceleration of the Universe is driven by a (quintessence) scalar field that has interactions with dark matter, leading to energy exchange between the two fluids as the Universe expands. Baryons and radiation are not coupled to the scalar field as such a coupling is strongly constrained by Solar system tests of gravity requiring $\beta_{\mathrm{baryons}}^2 \lesssim 10^{-5}$. The dynamical equations at the background level are given by

$$\ddot{\phi} + 3H\dot{\phi} + \frac{\mathrm{d}V(\phi)}{\mathrm{d}\phi} = \sqrt{\frac{2}{3}}\beta(\phi)\frac{\rho_{\mathrm{DM}}}{M_{\mathrm{Pl}}}, \qquad (9)$$

$$\dot{\rho}_{\mathrm{DM}} + 3H\rho_{\mathrm{DM}} = -\sqrt{\frac{2}{3}}\beta(\phi)\dot{\phi}\frac{\rho_{\mathrm{DM}}}{M_{\mathrm{Pl}}}, \qquad (10)$$

$$\dot{\rho}_{\mathrm{b}} + 3H\rho_{\mathrm{b}} = 0. \qquad (11)$$

Each model on this form is specified by a potential $V(\phi)$ and a coupling function $\beta(\phi)$. The mass of the scalar field ϕ is $\mathcal{O}(H_0)$ at the present time that means that the field does not cluster significantly. The gravitational force on the dark matter particles is therefore equivalent to a time-dependent Newton's constant

$$G_{\mathrm{eff}}^{\mathrm{DM}} = G\left(1 + \frac{4}{3}\beta^2(a)\right), \qquad (12)$$

where $\beta(a) = \beta(\phi(a))$ and $\phi(a)$ is the background solution for ϕ. The absence of a coupling to baryons means that there is no need for a screening mechanism to be consistent with local tests of gravity. Observations of the CMB places the strongest constraints on the model that constraints $\beta \lesssim 0.2$ (Casas et al. 2016).

For the models considered here (Baldi 2012), we have $\beta(\phi) = \beta_0 e^{\frac{\beta_1\phi}{M_{\mathrm{Pl}}}}$ and $V(\phi) = Ae^{-\frac{\alpha\phi}{M_{\mathrm{Pl}}}}$, where $A = 0.002\,18M_{\mathrm{Pl}}^4$, $\alpha = 0.08$, $\beta_1 = 0$ and $\beta_0 = 0.05$ (the EXP1 model) and $\beta_0 = 0.15$ (the EXP3 model). The scalar field is normalized such that $\phi(z = 0) = 0$.

3 METHODS

In this section, we describe the simulations and the generation of the halo catalogues we have used for our analysis.

3.1 The simulations

To study the effects of MG on galaxy haloes, we took advantage of a wide range of available simulations with different models.

In brief, we used four different sets of simulations, each set using its own initial conditions and cosmology. For each set of simulations, we use the ΛCDM run as a reference for the corresponding MG runs.

The first set of simulations, f512, uses 512^3 particles in an $L = 256\,h^{-1}$Mpc. The reference ΛCDM cosmology for this set of simulations is $(\Omega_{\mathrm{m}}, \Omega_\Lambda, h, \sigma_8) = (0.267, 0.733, 0.719, 0.80)$. The $f(R)$ simulations have $f_{R0} = 10^{-4}$ (F4), 10^{-5} (F5) and 10^{-6} (F6). The initial density fluctuations have been normalized by the CMB, which yields different σ_8 at $z = 0$.

The second set of simulations, f1024, uses 1024^3 particles in an $L = 1024\,h^{-1}$Mpc box. The reference cosmology is $(\Omega_{\mathrm{m}}, \Omega_\Lambda, h, \sigma_8) = (0.267, 0.733, 0.719, 0.80)$. The associated MG simulations is $f(R)$ models with $f_{R_0} = 10^{-5}$, but has been normalized to the same $\sigma_8 = 0.80$ at $z = 0$.

The above two sets of simulations were run using the ISIS code (Llinares et al. 2014), which is based on RAMSES (Teyssier 2002). The code used was recently compared to other MG codes (Winther et al. 2015) and for the two models studied here, $f(R)$ and DGP, excellent (sub-per cent) agreement was found in the enhancement of the matter matter power-spectrum relative to ΛCDM (both computed within each code) for scales $k \lesssim 5$–$10\,h$Mpc^{-1}. Similar per cent level agreement was found for the enhancement of the velocity divergence power spectrum, halo abundances and halo profiles for all redshifts studied $z \lesssim 2$.

The third set of simulation aims to study DGP gravity. The reference GR cosmology has $(\Omega_{\mathrm{m}}, \Omega_\Lambda, h) = (0.271, 0.729, 0.703)$, with 512^3 particles in an $L = 250\,h^{-1}$Mpc box, and was also run with ISIS. The DGP run was run with the crossover scale $r_c = 1.2/H_0$.

The fourth set of simulations comes from the publicly available L-CoDECS project (Baldi et al. 2010; Baldi 2012), a set of N-body simulations of coupled DE, evolving 2×1024^3 particles (dark matter and baryons without hydrodynamics) in an $L = 1000\,h^{-1}$Mpc box with the modified version of GADGET-2

Set	Name	Normal- ization	L (h^{-1}Mpc)	N
f512	ΛCDM	CMB	256	512^3
	F4	CMB	256	512^3
	F5	CMB	256	512^3
	F6	CMB	256	512^3
f1024	ΛCDM	$\sigma_8 = 0.8$	1024	1024^3
	F5	$\sigma_8 = 0.8$	1024	1024^3
DGP	ΛCDM	CMB	250	512^3
	DGP1.2	CMB	250	512^3
CoDECS	ΛCDM	CMB	1000	1024^3
	EXP1	CMB	1000	1024^3
	EXP3	CMB	1000	1024^3

(Springel 2005) by Baldi et al. (2010). The reference cosmology is $(\Omega_m, \Omega_\Lambda, h) = (0.2711, 0.7289, 0.703)$. We used two simulations: EXP1 and EXP3, which have an exponential scalar self-interaction potential with $\beta_0 = 0.05$ and 0.15, respectively. Note that to fairly compare the CoDECS simulations, which include baryons, with the N-body ones, we exclude the baryon particles from our the CoDECS simulations, and correct the mass of the CDM particles accordingly by Ω_m/Ω_{CDM}. The simulation parametres are summarized in Table 1.

We note that, since each set of simulations (f512, f1024, DGP and CoDECS) has different initial conditions and cosmologies, the results should not be compared between the sets, but within a given set between each model.

3.2 Halo detection and catalogues

The haloes and subhaloes were respectively detected as in L'Huillier et al. (2015) using the Ordinary Parallel Friend-of-Friend (OPFOF) and physically self-bound (PSB) algorithms (Kim & Park 2006). OPFOF is a memory-efficient parallel implementation of FOF and PSB is a subhalo finder that finds density peaks in a similar way to SUBFIND (Springel et al. 2001), and additionally truncates the subhaloes to the tidal radius. For more details, we refer the reader to Kim & Park (2006).

For consistency between different gravity models, we defined the virial radius R_{vir} as

$$\frac{M(<R_{vir})}{4/3\pi R_{vir}^3} = 200\rho_c(z), \tag{13}$$

where

$$\rho_c(z) = \frac{3H^2(z)}{8\pi G} \tag{14}$$

is the critical density of the Universe.[1]

PSB also calculates the potential energy and the tidal radius of each subhalo candidate before removing unbound particles. In this step, we also assume a Newtonian gravity in all cases. We expect this to slightly underestimate the bound masses in MG, by removing particles that are actually bound to the halo. This has been shown to slightly underestimate the mass function (Li & Zhao 2010).

[1] This definition is different from the one used in L'Huillier et al. (2015), and does not take into account the dependence of Δ_c with redshift, since the Bryan & Norman (1998) formula is only valid for a flat ΛCDM cosmology.

Targets consist of PSB sub-haloes with more than 50 particles, yielding a minimal mass of, respectively, 4.72×10^{11}, 3.78×10^{12}, 4.47×10^{11} and 3.57×10^{12} h^{-1}M$_\odot$ in the f512, f1024, DGP and CoDECS simulations. A target is defined to be interacting with a neighbour if it is located within twice the virial radius of its neighbour, and if the neighbour is at least 0.4 the mass of the target. We note that we slightly changed the definition of interactions with respect to L'Huillier et al. (2015, 2017) in order to increase our statistics.

In order to define the large-scale density, we calculated the density field ρ_{20} smoothed over the 20 nearest neighbours of each target halo (L'Huillier et al. 2015, 2017), and defined as

$$\rho_{20} = \sum_{i=1}^{20} M_i W(r_i, h), \text{ where} \tag{15}$$

$$W(r_i, h) = \frac{1}{\pi h^3} \begin{cases} 1 - \frac{3}{2}\left(\frac{r}{h}\right)^2 + \frac{3}{4}\left(\frac{r}{h}\right)^3, & 0 \leqslant \frac{r}{h} \leqslant 1 \\ \frac{1}{4}\left(2 - \left(\frac{r}{h}\right)\right)^3, & 1 \leqslant \frac{r}{h} \leqslant 2 \\ 0, & \frac{r}{h} \geqslant 2 \end{cases} \tag{16}$$

is the cubic spline kernel used in smoothed particle hydrodynamics (e.g. Monaghan & Lattanzio 1985), r_i is the distance to the ith neighbour and h is the smoothing length, defined as the distance to the 21st neighbour. The large-scale overdensity is thus defined as

$$1 + \delta_{20} = \frac{\rho_{20}}{\bar{\rho}_h}, \tag{17}$$

where $\bar{\rho}_h$ is the mean halo density.

4 SPIN AND SHAPE OF SUBHALOES IN MG

In this section, we present our results from a systematic analysis of the shape and spin parameters of PSB subhaloes in simulations of the MG and coupled DE theories.

4.1 Shapes

The internal distribution of matter can be described by the inertia tensor

$$I_{ij} = \sum_\alpha x_{\alpha,i} x_{\alpha,j}, \tag{18}$$

where $x_{\alpha,i}$ is the ith coordinate of particle α.

The sphericity s and oblateness q are defined as $q = \frac{b}{a}$ and $s = \frac{c}{a}$ where $a^2 > b^2 > c^2$ are the eigenvalues of I. We note that, in order to limit resolution effects, we only considered subhaloes resolved with more than 100 particles.

The first and second rows of Fig. 1, respectively, show the distribution of the oblateness q and sphericity s of PSB subhaloes in the f512 (first column), f1024 (second column), DGP (third column) and CoDECS (fourth column) sets of simulations. The solid lines show the distributions at $z = 0$ and the dashed lines at $z = 1$. The error bars show the Poisson error in each bin and the ΛCDM reference simulation in each set is shown in black.

In the first and second rows, $f(R)$ simulations seem to have a slightly lower sphericity and oblateness, especially at $z = 1$. In the case of $f(R)$ gravity, the difference between the distributions is larger at $z = 1$ than $z = 0$. In the DGP simulation, we find no difference on the distribution of the shape parameters compared to ΛCDM. In interacting DE models, the (weakly coupled) EXP1 model is indistinguishable from GR, while the (more strongly coupled) EXP3 model has a slightly larger median sphericity and oblateness. However, the
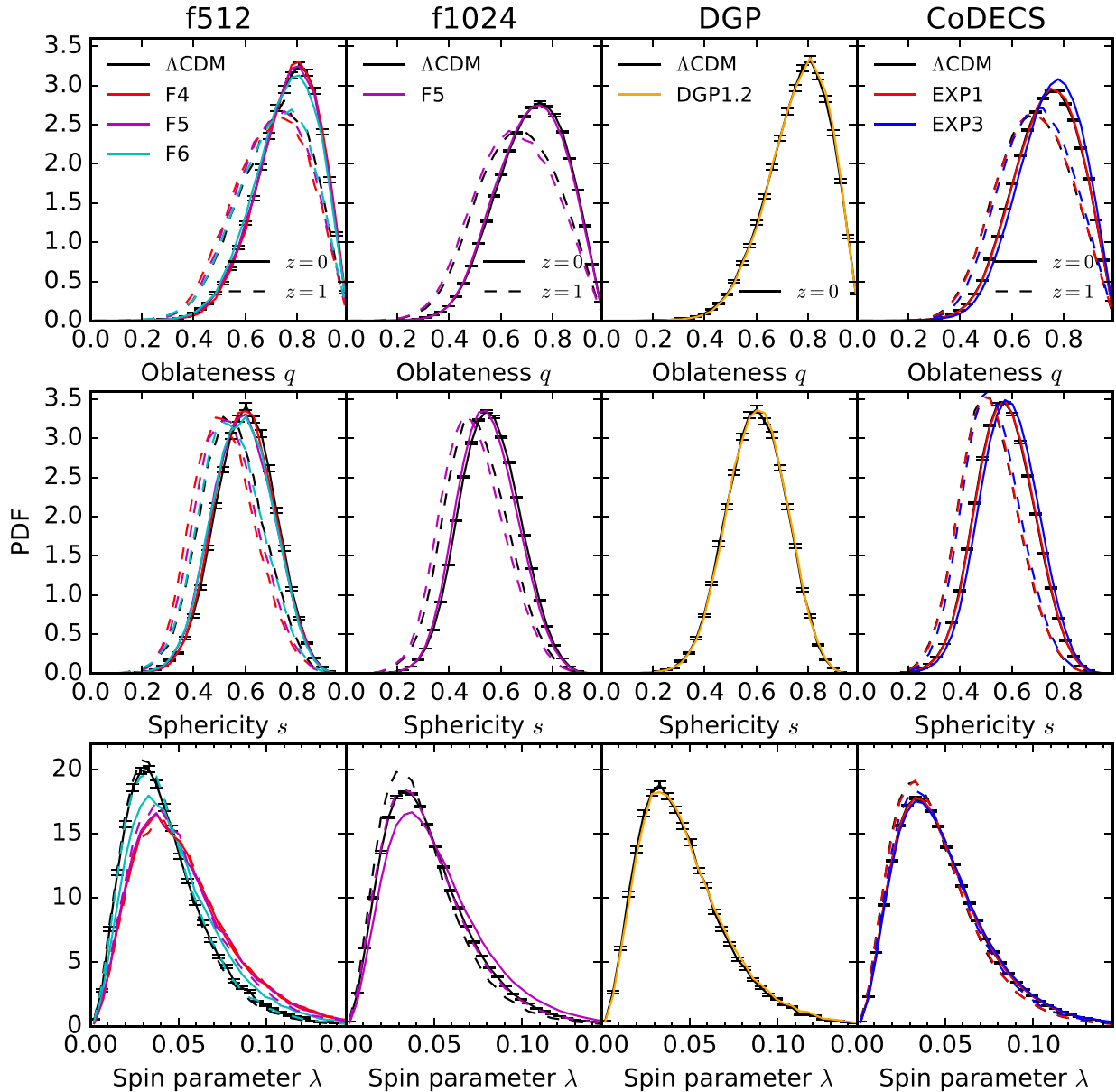
Figure 1. Distribution of the oblateness (top), sphericity (middle) and spin (bottom) parameters in the four sets of simulations. The solid lines show the results at $z = 0$ and the dashed ones at $z = 1$. The ΛCDM results are in black. $f(R)$ yields a lower sphericity, oblateness, and a larger Bullock spin parameter. There is no sign for departure from GR in DGP. Coupled DE with large coupling (EXP3) yields larger oblateness and sphericity than GR, but show no deviation for the spin parameters.

shift is very small. For instance, in the case of CoDECS, the median and 68 per cent percentile of the oblateness q are $0.7561^{+0.0589}_{-0.0629}$ and $0.7406^{+0.0615}_{-0.0652}$ for EXP3 and ΛCDM at $z = 0$.

4.2 Spin parameter

To describe the rotation of haloes, we calculated the spin parameters of each PSB subhalo, defined as (Bullock et al. 2001)

$$\lambda_B = \frac{|\boldsymbol{J}|}{\sqrt{2}MRV}, \tag{19}$$

where

$$V^2 = \frac{GM}{R}, \tag{20}$$

and $\boldsymbol{J}$ is the sum of the angular momenta of each particle in the halo.

In the third row of Fig. 1, we show the spin distribution of the spin parameters. We only consider haloes resolved with more than 100 particles. In $f(R)$ gravity, the fifth force tends to speed up halo rotation in agreement with Lee et al. (2013). On the other hand, DGP and coupled DE seem to have no effect on the spin distribution.

However, the effect of MG on the distribution of the structural parameters is overall very small. For instance, the median, 16th, and 84th percentiles associated with the spin parameter at $z = 0$ in the f1024 set is $0.0425^{+0.0122}_{-0.0101}$ and $0.0467^{+0.0136}_{-0.0112}$ for the ΛCDM and F5 models, respectively, making the effect of MG on the spin distribution difficult to detect observationally.

Fig. 2 shows the mass dependence of the spin distribution at $z = 0$ in two mass bins, namely $l_M < 14.30$ (top) and $l_M > 14.30$ (bottom),
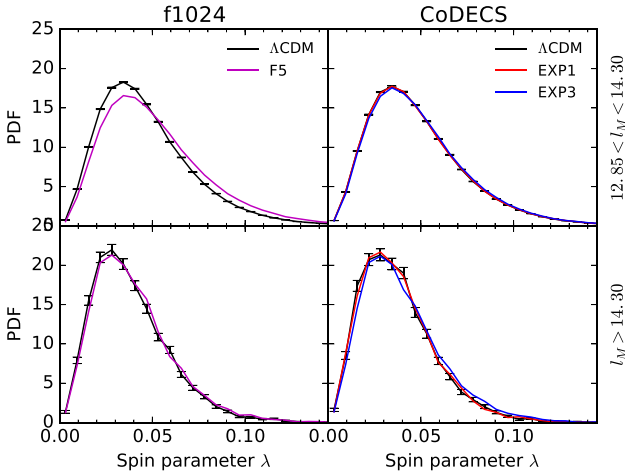
Figure 2. Spin distribution at $z = 0$ for $l_M < 14.30$ (top) and $l_M > 14.30$ (bottom), where $l_M = \log_{10} hM/M_\odot$.

where $l_M = \log_{10} hM/M_\odot$. In the CoDECS simulations, as expected, the coupled DE models show no difference with ΛCDM at any mass bins. However, in the lower mass bin, the spin distribution of F5 is shifted towards larger spins with respect to that of ΛCDM, while no difference can be seen in the higher mass bin. Again, this can be understood as an effect of screening of the fifth force at high masses. We note that Carlesi et al. (2014) studied interacting DE models in higher resolution simulations, and found that interacting DE affects the spin at lower halo masses.

5 EFFECTS OF MG ON HALO INTERACTIONS

In this section, we study the rate of close interactions ($<2R_{vir}$) and their effects on the alignment of the spins of the interacting pair.
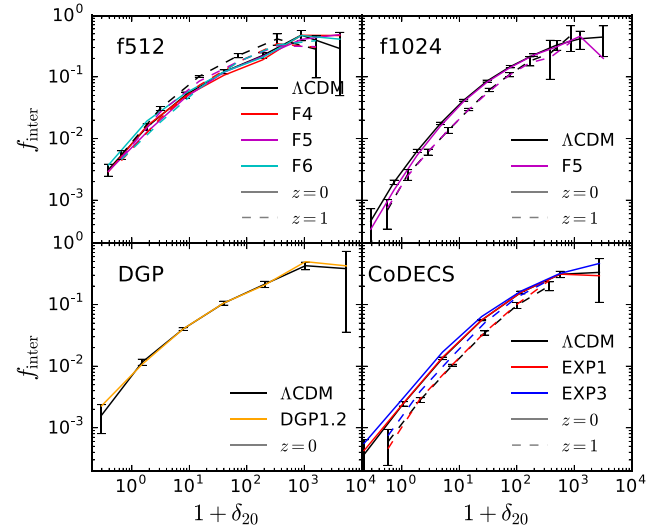
5.1 Interaction rate

The interaction rate depends on the mass function and the subhalo mass function, which in turn depend on the gravity model. Fig. 3a shows the interaction rates in different gravity models as a function of mass for each set of simulations. The interaction rate is defined as the fraction of targets undergoing an interaction with respect to the total number of targets in the considered bin. We divided the simulation volume in eight equal cubes, and calculated the mean and standard deviation of the interaction rate in each bin of mass and density. For the sake of readability, we only plot the error-bars for GR, since the other gravity models yield similar uncertainties.

The decreasing shape of the interaction rate as a function of mass is a consequence of our definition: more massive haloes are less likely to be interacting with a more massive halo (L'Huillier et al. 2015). The f512 and DGP simulations have large statistical fluctuations, due to their small volumes, making it difficult to draw any conclusion. The other sets of simulations, f1024 and CoDECS, have larger box sizes, and thus better statistics. In coupled DE simulations, the interaction rate between EXP1 and GR are consistent within the error-bars, while EXP3 has a higher interaction rate in the whole range. F5 yields a very similar interaction rate to GR.

Fig. 3b shows the interaction rate as a function of the large-scale density $1 + \delta_{20}$ for each set of simulation. Again, the results from small-box simulations (f512 and DGP) are consistent within their large error-bars. The tighter error-bars in f1024 show that the interaction rate dependence on the large-scale density δ_{20} is not
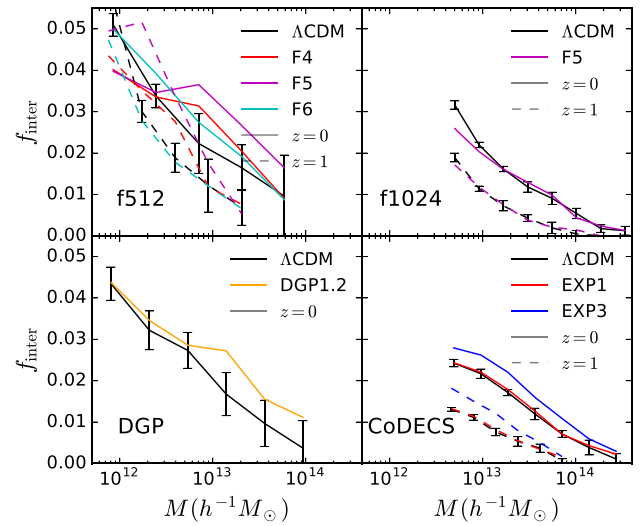
(a) Interaction rate as a function of mass.

(b) Interaction rate as a function of density.

Figure 3. Interaction rate as a function of mass (a) and density (b) for our different MG and DE models.

affected by $f(R)$ gravity. In the coupled DE, however, while EXP1 agrees with GR, at all redshift and density, the interaction fraction in EXP3 is systematically higher than in GR for $2 \simeq 1 + \delta_{20} \simeq 100$ at $z = 1$ and $1 \simeq 1 + \delta_{20} \simeq 20$ at $z = 0$. The excess of interactions is larger at $z = 1$ than at $z = 0$. However, in this regime, the interaction fraction is very low (<0.1), which makes it difficult to test observationally.

5.2 Effects of MG on the alignments of interacting pairs

In this section, we study the effects of MG on the alignment of the spins of interacting targets at $z = 0$. In L'Huillier et al. (2017), we showed that interacting haloes show a strong alignment, and the strength of the signal increases with mass, and only weakly depends on density.

5.2.1 Characterization of the alignment signal

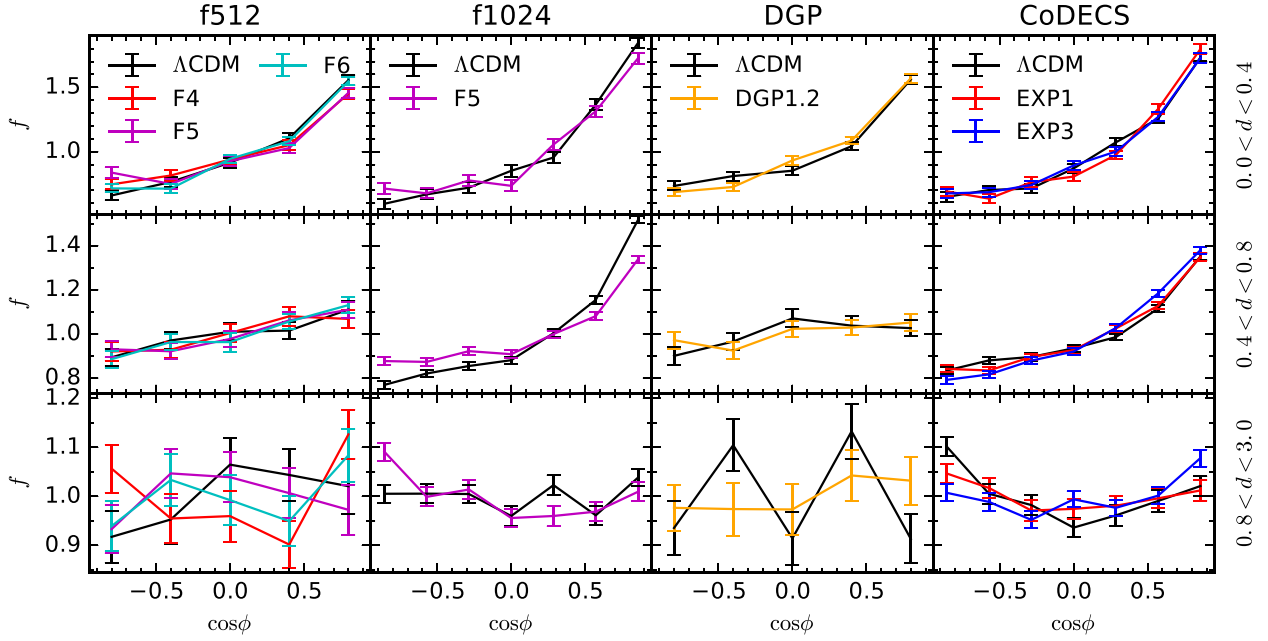Following Brainerd (2005), Yang et al. (2006) and L'Huillier et al. (2017) in order to quantify the alignment of an angle θ between any

Figure 4. Normalized pair count of $\cos\phi$, where $\phi = (\boldsymbol{J}_{\mathrm{T}}, \boldsymbol{J}_{\mathrm{N}})$ as a function of the pair separation d/d_1, where $d_1 = 1\,h^{-1}\mathrm{Mpc}$, at $z = 0$. The pair separation increases from the top to bottom row. In the second column, F5 shows a weaker alignment than GR for $0.4 < d/d_1 < 0.8$.

two vectors $(\boldsymbol{u}, \boldsymbol{v})$, we proceed as follow. For a given bin of $\cos\theta$, we count the number of pairs in this bin $N(\theta)$. We then randomly shuffle the pairs 100 times, and calculate the mean and standard deviation $\langle N(\theta)\rangle$ and σ_θ. We then define the normalized pair count as

$$f(\theta) = \frac{N(\theta)}{\langle N(\theta)\rangle}. \tag{21}$$

The error is then given by $\sigma_\theta/\langle N(\theta)\rangle$. Random configurations have $f(\theta) = 1$, while alignment have $f(\cos\theta \simeq \pm 1) \gg 1$, and anti-aligned (orthogonal) configurations have $f(\cos\theta \simeq 0) \gg 1$.

5.2.2 Results

Fig. 4 shows the normalized pair count $f(\phi)$, where $\phi = (\boldsymbol{J}_{\mathrm{T}}, \boldsymbol{J}_{\mathrm{N}})$, and T and N denote the target and neighbour halo, respectively, in the different simulation sets. We divided each sample into three bins of separation $0 < d < 0.4\,h^{-1}\mathrm{Mpc}$ (top), $0.4 < d < 0.8\,h^{-1}\mathrm{Mpc}$ (middle) and $0.8 < d < 3\,h^{-1}\mathrm{Mpc}$ (bottom).

In the lower panels, for $d > 0.8\,h^{-1}\mathrm{Mpc}$, the alignment is consistent with a random alignment for each model, showing no difference between MG, DE and GR. The alignment becomes stronger as the pair separation decreases, as expected from stronger tidal forces, and from previous studies on the spin correlation function (e.g. Singh, Mandelbaum & More 2015).

In the f512 and DGP simulations, the small statistics coming from the small box size do not allow us to see any deviation from GR. For f1024 (second column), at $0.4 < d < 0.8\,h^{-1}\mathrm{Mpc}$, the alignment signal in F5 is weaker than in GR (larger excess of pairs with $\cos\phi \simeq 1$ and lower for $\cos\phi \simeq -1$). For $d \leq 0.4\,h^{-1}\mathrm{Mpc}$, the alignments become consistent again, showing almost no deviation from GR. This can be understood as the action of the fifth force in the F5 model at intermediate separations ($0.4 < d < 0.8\,h^{-1}\mathrm{Mpc}$), yielding a weaker alignment. For small separations, the fifth force is screened and the alignment signal becomes consistent with ΛCDM. No such behaviour is seen in CoDECS, where the alignment signal is consistent with ΛCDM for all separations. This is consistent with

Fig. 1, where no effect of DE on the spin distribution could be detected.

6 ALIGNMENT WITH THE LARGE-SCALE STRUCTURE

In the previous section, we considered the small-scale alignment of pairs of interacting haloes. In this section, we are interested in the alignment of the spin of dark matter haloes and the large-scale structures, or large-scale alignment.

Alignment of the shapes and spins of haloes with the large-scale structures have been studied deeply in the literature (e.g. Hahn et al. 2007; Zhang et al. 2009; Codis et al. 2012; Libeskind et al. 2013a; Trowland, Lewis & Bland-Hawthorn 2013; Zhang et al. 2013; Forero-Romero, Contreras & Padilla 2014; Zhang et al. 2015).

There are several ways to characterize the cosmic web. We used the tidal tensor (Hahn et al. 2007; Forero-Romero et al. 2009) and defined the large-scale structure as follows. The matter density field $\delta(\boldsymbol{x})$ is calculated using a count-in-cell assignment scheme. The smooth density field $\tilde{\delta}_R$ was then obtained by smoothing the matter density with a Gaussian kernel of radius $R_{\mathrm{G}} = 4\,h^{-1}\mathrm{Mpc}$. We then calculated the tidal tensor $\boldsymbol{T}$, defined as

$$T_{ij} = \frac{\partial^2 \tilde{\phi}}{\partial x_i \partial x_j}, \tag{22}$$

where $\tilde{\phi}$ is the gravitational potential, solution to the Poisson equation (assuming GR)

$$\nabla^2 \tilde{\phi} = \tilde{\delta}_R. \tag{23}$$

We then calculated the eigenvalues of $\boldsymbol{T}$, $\lambda_1 \leq \lambda_2 \leq \lambda_3$, and defined voids, walls, filaments and knots pixels with, respectively, 0, 1, 2 and 3 eigenvalues larger than $\lambda_{\mathrm{thresh}}$. We set $\lambda_{\mathrm{thresh}} = 0.4$, which visually provided the best cosmic web. A discussion about the choice of $\lambda_{\mathrm{thresh}}$ may be found in Forero-Romero et al. (2009) and Alonso, Eardley & Peacock (2015). This calculation was made using the
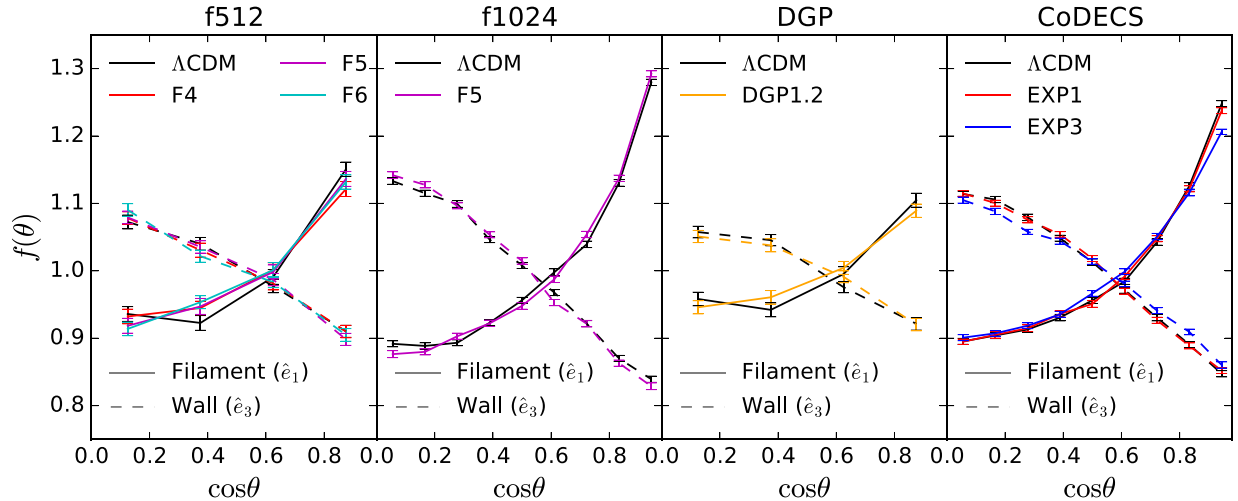
Figure 5. Alignment of the major axis with the large-scale structures. Shown is the normalized pair count $f(\theta_i)$, where $\theta_i = (\boldsymbol{a}_\mathrm{T}, \hat{e}_i)$ is the angle between the major axis of the target and the direction of the wall (θ_3) or filament (θ_1).

DENSTOOLS code[2]. Each pixel thus has an unambiguously defined environment (void, wall, filament, knot). For each halo, we define the environment as that of the pixel where its centre is located.

Fig. 5 shows the normalized pair count $f(\theta_i)$ (equation 21), where $\theta_i = (\boldsymbol{a}_\mathrm{T}, \hat{e}_i)$ is the angle between the major axis of the halo and the direction of the LSS ($\hat{e}_3$ is the direction normal to the walls and $\hat{e}_1$ the direction of the filaments). Since knots and voids do not have a well-defined direction, we exclude them from this analysis.

The major axis is well aligned with the direction of the filaments, and in the plane of the wall (orthogonal to the normal direction of the wall), confirming previous findings (e.g. Zhang et al. 2009). EXP3 shows the strongest deviation to GR, with weakly but systematically weaker alignment signal than GR. EXP1 on the other hand shows no deviation at all.

In the f1024 simulations, F5 seems to show a stronger alignment than GR, although the significance is weak. A similar trend can be seen in F256 and DGP, where $f(R)$ models seem to show stronger alignment than GR, while DGP seem to show weaker alignment than GR. However, in f512 and DGP, the large error-bars do not allow strong conclusions.

7 SUMMARY AND DISCUSSION

Using cosmological *N*-body simulations with different gravity models, namely ΛCDM, $f(R)$, DGP and coupled DE, we studied the effect of gravity and DE on internal properties of subhaloes, namely structural and spin parameters. We also studied the effects of MG on the halo interaction rate.

We then studied the alignment of the spins of interacting pairs, following L'Huillier et al. (2017). Finally, we performed for the first time a systematic study of the alignment of haloes with the large-scale structures (filaments and walls) in MG, as well as of the distribution of the spin parameters in voids and knots. Our findings are summarized below:

(i) $f(R)$ models yield a larger Bullock spin parameter in agreement with Lee et al. (2013) and a lower oblateness and sphericity. At $z = 0$, the difference in the structural parameters (q and s) is smaller than at $z = 1$.

(ii) EXP3 yields larger oblateness and sphericity, while the spin parameter is unaffected. EXP1 is essentially indistinguishable from GR.

(iii) The interaction rate is largely unaffected by MG. Strongly coupled DE models however show an enhancement of the interaction rate at all masses.

(iv) The alignment of the spins of interacting pairs of haloes decreases with the pair separation for each model. In F5, the a alignment is similar to GR for $d < 0.4\,h^{-1}\mathrm{Mpc}$, and becomes weaker for $0.4 < d < 0.8\,h^{-1}\mathrm{Mpc}$, due to the effect of the fifth force. Coupled DE does not affect the spin alignment of pairs.

(v) The (anti-)alignment of the major axis of haloes with the direction of the filaments (walls) is weaker for the EXP3 model than in GR. Simulations with $L \simeq 250\,h^{-1}\mathrm{Mpc}$ do not show any departure from GR.

(vi) Large volumes ($L \simeq 1\,h^{-1}\mathrm{Gpc}$) are needed to distinguish between gravity models.

The fact that very large volumes are needed to detect any deviation from GR shows the weakness of the signal. For instance, in the case of the alignment with the LSS, the large-scale alignment is largely unaffected by MG. Therefore, one can argue that treatments of intrinsic alignment based on GR should not induce bias in the analysis.

The strength of our study is to apply the same method to several sets of simulations with different gravity models, box size and resolutions. This is the first study devoted to the study of the small- and large-scale alignment in MG and DE models.

REFERENCES

Alonso D., Eardley E., Peacock J. A., 2015, MNRAS, 447, 2683
Amendola L., 2000, Phys. Rev. D, 62, 043511
Amendola L. et al., 2013, Living Rev. Relativ., 16, 6

[2] The code is available at https://github.com/damonge/DensTools.

Baldi M., 2012, MNRAS, 422, 1028

Baldi M., Pettorino V., Robbers G., Springel V., 2010, MNRAS, 403, 1684

Brainerd T. G., 2005, ApJ, 628, L101

Brax P., van de Bruck C., Davis A.-C., Shaw D. J., 2008, Phys. Rev. D, 78, 104021

Bryan G. L., Norman M. L., 1998, ApJ, 495, 80

Bullock J. S., Dekel A., Kolatt T. S., Kravtsov A. V., Klypin A. A., Porciani C., Primack J. R., 2001, ApJ, 555, 240

Carlesi E., Knebe A., Lewis G. F., Wales S., Yepes G., 2014, MNRAS, 439, 2943

Casas S., Amendola L., Baldi M., Pettorino V., Vollmer A., 2016, J. Cosmol. Astropart. Phys., 1, 045

Clifton T., Ferreira P. G., Padilla A., Skordis C., 2012, Phys. Rep., 513, 1

Codis S., Pichon C., Devriendt J., Slyz A., Pogosyan D., Dubois Y., Sousbie T., 2012, MNRAS, 427, 3320

Colless M., 1999, Phil. Trans. R. Soc. A, 357, 105

Copeland E. J., Sami M., Tsujikawa S., 2006, Int. J. Mod. Phys. D, 15, 1753

De Felice A., Tsujikawa S., 2010, Living Rev. Relativ., 13, 3

Dvali G., Gabadadze G., Porrati M., 2000, Phys. Lett. B, 485, 208

Forero-Romero J. E., Hoffman Y., Gottlöber S., Klypin A., Yepes G., 2009, MNRAS, 396, 1815

Forero-Romero J. E., Contreras S., Padilla N., 2014, MNRAS, 443, 1090

Gannouji R., Moraes B., Mota D. F., Polarski D., Tsujikawa S., Winther H. A., 2010, Phys. Rev. D, 82, 124006

Gill S. P. D., Knebe A., Gibson B. K., 2004, MNRAS, 351, 399

Hahn O., Carollo C. M., Porciani C., Dekel A., 2007, MNRAS, 381, 41

Hellwing W. A., Cautun M., Knebe A., Juszkiewicz R., Knollmann S., 2013, J. Cosmol. Astropart. Phys., 10, 012

Hu W., Sawicki I., 2007, Phys. Rev. D, 76, 064004

Joyce A., Jain B., Khoury J., Trodden M., 2015, Phys. Rep., 568, 1

Khoury J., 2010, preprint (arXiv:1011.5909)

Kim J., Park C., 2006, ApJ, 639, 600

Kim J., Park C., L'Huillier B., Hong S. E., 2015, J. Korean Astron. Soc., 48, 213

Knollmann S. R., Knebe A., 2009, ApJS, 182, 608

Koivisto T., 2005, Phys. Rev. D, 72, 043516

Koivisto T., Mota D. F., 2007, Phys. Lett. B, 644, 104

L'Huillier B., Park C., Kim J., 2015, MNRAS, 451, 527

L'Huillier B., Park C., Kim J., 2017, MNRAS, 466, 4875

Laureijs R. et al., 2011, preprint (arXiv:1110.3193)

Lee J., Zhao G.-B., Li B., Koyama K., 2013, ApJ, 763, 28

Leithes A., Malik K. A., Mulryne D. J., Nunes N. J., 2016, preprint (arXiv:1608.00908)

Li B., 2011, MNRAS, 411, 2615

Li B., Zhao H., 2010, Phys. Rev. D, 81, 104047

Li B., Mota D. F., Barrow J. D., 2011, ApJ, 728, 109

Li B., Zhao G.-B., Koyama K., 2012, MNRAS, 421, 3481

Libeskind N. I., Hoffman Y., Forero-Romero J., Gottlöber S., Knebe A., Steinmetz M., Klypin A., 2013a, MNRAS, 428, 2489

Libeskind N. I., Hoffman Y., Steinmetz M., Gottlöber S., Knebe A., Hess S., 2013b, ApJ, 766, L15

Llinares C., Mota D. F., 2013a, Phys. Rev. Lett., 110, 151104

Llinares C., Mota D., 2013b, Phys. Rev. Lett., 110, 161101

Llinares C., Mota D. F., Winther H. A., 2014, A&A, 562, A78

Maartens R., Koyama K., 2010, Living Rev. Relativ., 13, 5

Monaghan J. J., Lattanzio J. C., 1985, A&A, 149, 135

Mota D. F., Kristiansen J. R., Koivisto T., Groeneboom N. E., 2007, MNRAS, 382, 793

Mota D. F., Shaw D. J., Silk J., 2008, ApJ, 675, 29

Mota D. F., Sandstad M., Zlosnik T., 2010, J. High Energy Phys., 12, 051

Peebles P. J. E., 1969, ApJ, 155, 393

Perlmutter S. et al., 1998, Nature, 391, 51

Pettorino V., 2013, Phys. Rev. D, 88, 063519

Riess A. G. et al., 1998, AJ, 116, 1009

Sabiu C. G., Mota D. F., Llinares C., Park C., 2016, A&A, 592, A38

Shi D., Li B., Han J., Gao L., Hellwing W. A., 2015, MNRAS, 452, 3179

Singh S., Mandelbaum R., More S., 2015, MNRAS, 450, 2195

Springel V., 2005, MNRAS, 364, 1105

Springel V., White S. D. M., Tormen G., Kauffmann G., 2001, MNRAS, 328, 726

Teyssier R., 2002, A&A, 385, 337

Trowland H. E., Lewis G. F., Bland-Hawthorn J., 2013, ApJ, 762, 72

Wetterich C., 1995, A&A, 301, 321

Will C. M., 2006, Living Rev. Relativ., 9, 3

Will C. M., 2014, Living Rev. Relativ., 17, 4

Winther H. A. et al., 2015, MNRAS, 454, 4208

Yang X., van den Bosch F. C., Mo H. J., Mao S., Kang X., Weinmann S. M., Guo Y., Jing Y. P., 2006, MNRAS, 369, 1293

Zhang Y., Yang X., Faltenbacher A., Springel V., Lin W., Wang H., 2009, ApJ, 706, 747

Zhang Y., Yang X., Wang H., Wang L., Mo H. J., van den Bosch F. C., 2013, ApJ, 779, 160

Zhang Y., Yang X., Wang H., Wang L., Luo W., Mo H. J., van den Bosch F. C., 2015, ApJ, 798, 17

Zhao G.-B., Li B., Koyama K., 2011, Phys. Rev. Lett., 107, 071303

APPENDIX A: PEEBLES VERSUS BULLOCK SPINS

In this section, we show how the definition of the spin parameter is affected by MG. Peebles (1969) defined the spin parameter as

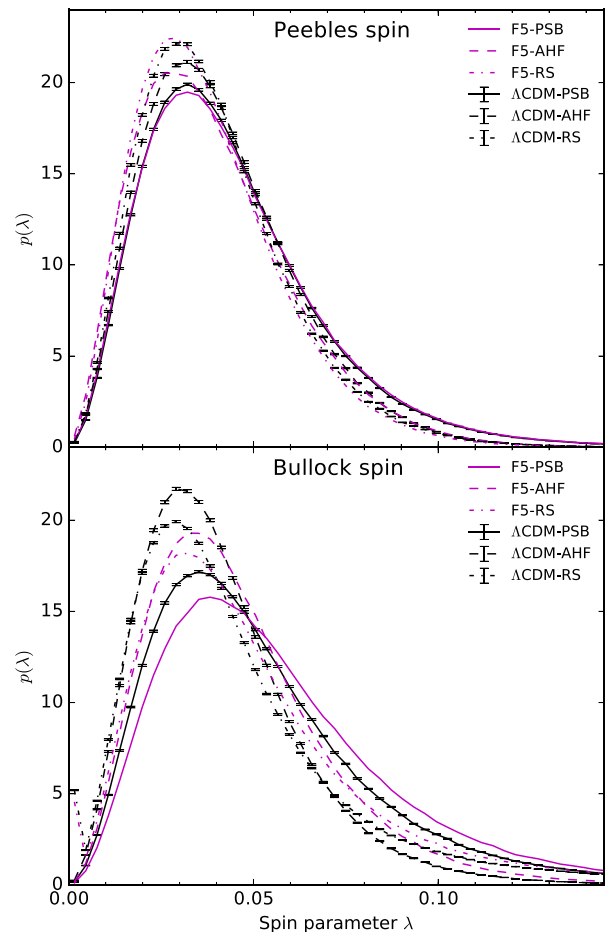$$\lambda_{\rm P} = \frac{|\mathbf{J}|\sqrt{|E|}}{GM^{5/2}}, \tag{A1}$$

Figure A1. PDF of the Peebles (top) and Bullock (bottom) spin parameters for f1024 GR (black) and F5 (magenta) at $z = 0$, and for PSB (solid), AHF (dashed) and ROCKSTAR (dash–dotted) lines.

where $E = W + K$ is the total (kinetic plus potential) energy.[3]

Fig. A1 compares the distributions of the Peebles and Bullock's parameters in MG. In the Peebles definition, the energy is calculated assuming GR, which underestimates the actual energy of the halo, yielding a lower value of the spin parameter in MG.

We also show the effect of the halo-finder on the spin computation. For that purpose, we used AHF (Gill, Knebe & Gibson 2004; Knollmann & Knebe 2009) to detect spherically overdense haloes. Moreover, the difference in the Peebles parameter between PSB and AHAHFF/ROCKSTAR can be understood by the following consideration. PSB assumes a Plummer gravitational potential while calculating the potential energy, which is used for the unbinding step as well as the computation of the spin parameter. AHF and ROCKSTAR, however,

assume a Newtonian potential. Regarding the difference in the Bullock spin, PSB defines the radius of a subhalo as a function of the mass only, via equation (13), while AHF and ROCKSTAR define it as the distance to the furthest particle. Regardless of the differences, the trend is consistent between both definitions of the spin parameter: $f(R)$ gravity yields a larger Bullock spin and has little effect on the Peebles spin.

---

[3] Note that in case of MG, we calculated E assuming GR.

This paper has been typeset from a TEX/LATEX file prepared by the author.